

# DreamAnywhere: Object-Centric Panoramic 3D Scene Generation

EDOARDO A. DOMINICI, Huawei Technologies, Switzerland

JOZEF HLADKY, Huawei Technologies, Germany

FLOOR VERHOEVEN, Huawei Technologies, Switzerland

LUKAS RADL, Graz University of Technology, Austria

THOMAS DEIXELBERGER, Huawei Technologies, Austria

STEFAN AINETTER, Huawei Technologies, Austria

PHILIPP DRESCHER, Huawei Technologies, Austria

STEFAN HAUSWIESNER, Huawei Technologies, Austria

ARNO COOMANS, Huawei Technologies, Switzerland

GIACOMO NAZZARO, Huawei Technologies, Switzerland

KONSTANTINOS VARDIS, Huawei Technologies, Switzerland

MARKUS STEINBERGER, Graz University of Technology and Huawei Technologies, Austria

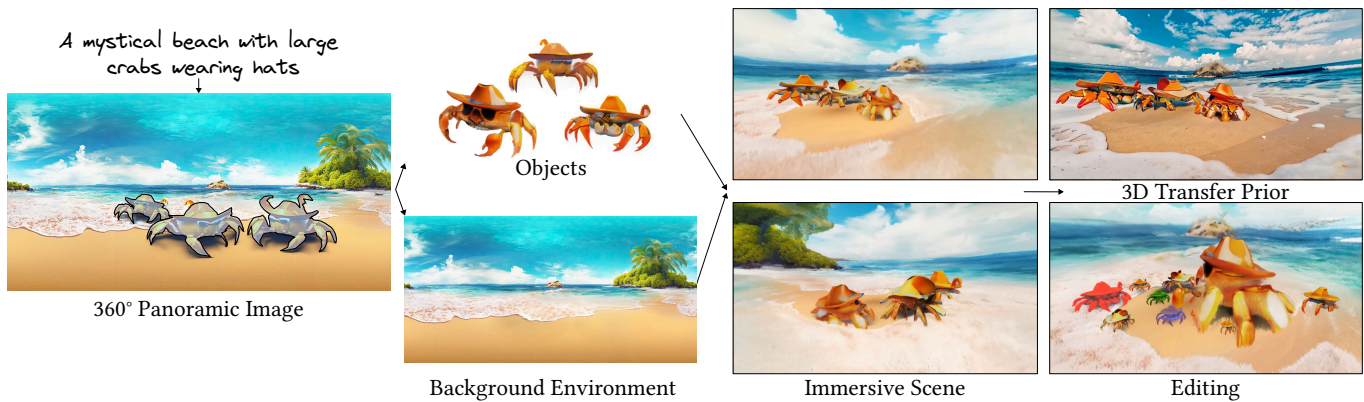


Fig. 1. Starting from a text prompt, our method generates 3D scenes leveraging a 360° panoramic image as intermediate representation to extract, reconstruct and compose objects in the environment. Our scenes, represented as 3D Gaussian splats, support long-range exploration and have high structural coherence even under large camera offsets. This improves immersive scene generation for existing applications, enables intuitive object-level editing and makes them strong 3D priors for world-to-world transfer models [Alhaija et al. 2025].

Recent advances in text-to-3D scene generation have demonstrated significant potential to transform content creation across multiple industries. Although the research community has made impressive progress in addressing the challenges of this complex task, existing methods often generate environments that are only front-facing, lack visual fidelity, exhibit limited scene understanding, and are typically fine-tuned for either indoor or outdoor settings. In this work, we address these issues and propose *DreamAnywhere*, a modular system for the fast generation and prototyping of 3D scenes. Our system synthesizes a 360° panoramic image from text, decomposes it into

Authors' addresses: Edoardo A. Dominici, Huawei Technologies, Switzerland, edoaramis@gmail.com; Jozef Hladky, Huawei Technologies, Germany, jozef.hladky@huawei.com; Floor Verhoeven, Huawei Technologies, Switzerland, floor.verhoeven@huawei.com; Lukas Radl, Graz University of Technology, Austria, lukas.radl@tugraz.at; Thomas Deixelberger, Huawei Technologies, Austria, thomas.deixelberger@huawei.com; Stefan Ainetter, Huawei Technologies, Austria, stefan.ainetter@huawei.com; Philipp Drescher, Huawei Technologies, Austria, philipp.drescher@huawei.com; Stefan Hauswiesner, Huawei Technologies, Austria, stefan.hauswiesner@huawei.com; Arno Coomans, Huawei Technologies, Switzerland, arno.coomans@huawei.com; Giacomo Nazzaro, Huawei Technologies, Switzerland, giacomo.nazzaro@huawei.com; Konstantinos Vardis, Huawei Technologies, Switzerland, konstantinos.vardis@huawei.com; Markus Steinberger, Graz University of Technology and Huawei Technologies, Austria, steinberger@tugraz.at.

background and objects, constructs a complete 3D representation through hybrid inpainting, and lifts object masks to detailed 3D objects that are placed in the virtual environment. *DreamAnywhere* supports immersive navigation and intuitive object-level editing, making it ideal for scene exploration, visual mock-ups, and rapid prototyping—all with minimal manual modeling. These features make our system particularly suitable for low-budget movie production, enabling quick iteration on scene layout and visual tone without the overhead of traditional 3D workflows. Our modular pipeline is highly customizable as it allows components to be replaced independently. Compared to current state-of-the-art text- and image-based 3D scene generation approaches, *DreamAnywhere* shows significant improvements in coherence in novel view synthesis and achieves competitive image quality, demonstrating its effectiveness across diverse and challenging scenarios. A comprehensive user study demonstrates a clear preference for our method over existing approaches, validating both its technical robustness and practical usefulness.

CCS Concepts: • **Computing methodologies** → **Artificial intelligence**; *Graphics systems and interfaces*.

Additional Key Words and Phrases: 3D scene generation, text-to-scene, diffusion models

## 1 INTRODUCTION

Generating large and immersive virtual 3D scenes from text remains a significant challenge with transformative applications in movie production, gaming, virtual reality, and simulation. Recent advances in generative modeling have led to impressive results but the 3D scenes are only coherent within small ranges of camera movement, resulting in incomplete structures and hallucinations when viewers attempt to explore beyond narrow boundaries.

Existing text-to-3D approaches leverage the richness and stylistic diversity of internet-scale diffusion models for progressive outpainting [Höllerin et al. 2023] or distillation sampling [Li et al. 2025; Shriram et al. 2024], but struggle to capture global coherence, leading to increasing semantic drift and structural collapse due to the difficulty of integrating depth estimates into a single 3D scene representation. Video diffusion models have been combined with large reconstruction models [Chen et al. 2025b; Yu et al. 2024c] but still face limitations in generating complete scenes observable from vastly different viewpoints maintaining coherency. Panoramic 360° images are an inherently good starting point for immersive viewing, in fact [Li et al. 2024; Zhou et al. 2024a] combine panoramic images with inpainting to enable parallax effects when moving away from the origin, further extended to multiple layers by [Yang et al. 2024c]. Similarly, approaches designed for 2D fly-throughs [Fridman et al. 2024; Liu et al. 2021; Yu et al. 2024a,b] can create visually convincing animations, but lack the global 3D structure required for full scene exploration.

Whilst large-scale and artistic 3D scene data remains scarce, there exists a wealth of 3D data for individual objects, offering a valuable resource for compositional approaches. Moreover, decomposing a 3D environment into individual entities offers important advantages for downstream applications [Armeni et al. 2019; Tulsiani et al. 2018]. If the layout and description of objects in a scene are known or provided manually, immersive scenes can be generated [Li et al. 2025]. However, optimizing scene layouts end-to-end continues to be a major challenge [Epstein et al. 2024; Zhang et al. 2023c].

Building on these insights, we present *DreamAnywhere*, a text-to-3D generation framework that leverages 360° panoramic image generation to drive scene style and geometry, while decomposing scenes into individual objects to preserve structural coherence and enable the generation of navigable 3D environments.

Our *main contribution* is a unified, modular system for 3D scene generation, enabled by the following key components:

- A panoramic image generation method that jointly fine-tunes a 360° image diffusion model with a perspective conditioning mechanism, improving out-of-domain sampling.
- A high-quality object reconstruction method that first synthesizes a detailed reference image from multimodal cues—textual, geometric, and stylistic—and then leverages it to guide robust 3D model generation and alignment, even for low-quality and incomplete segmented inputs.
- A hybrid inpainting strategy that combines 2D and 3D techniques: large-scale holes resulting from object removal are inpainted in the 360° image for global coherence, while smaller disocclusions caused by the 3D projection are addressed with 3D inpainting.

To evaluate our approach, we conduct both quantitative comparisons and a controlled user study, demonstrating that our method achieves superior quality, especially under large view offsets. Furthermore, qualitative results and user feedback indicate that our approach yields much more coherent and immersive scenes. As shown in Figure 1, this holds even for diverse camera movements.

## 2 RELATED WORK

Our 3D scene generation work lies at the intersection of image-based generation and compositional scene synthesis, bridging recent advances in both areas. For an in-depth discussion we refer readers to recent surveys on scene generation [Li et al. 2023; Tang et al. 2025] and object generation [Li et al. 2023; Po et al. 2024], and below we highlight the key developments most relevant to our approach.

### 2.1 Image-based Scene Generation

A successful line of work in image-based scene generation focuses on monolithic representations, where the entire scene is captured in a single unified 3D structure. A common technique involves iterative outpainting with image diffusion models to progressively extend the scene along a camera trajectory [Fridman et al. 2024; Höllerin et al. 2023; Liang et al. 2024; Yu et al. 2024a,b]. Although effective to some extent, these methods often suffer from the accumulation of visual artifacts and distortions across iterations, and offer limited flexibility for isolating and manipulating individual scene components.

An alternative set of techniques reconstructs 3D scenes from 2D images using inpainting-based methods, which lift partial views into 3D and fill occluded regions through inpainting [Shriram et al. 2024; Zhang et al. 2023b]. Although these reconstructions can appear photorealistic from specific angles, their quality tends to degrade when viewed from arbitrary viewpoints.

More recently, panorama-based approaches such as PanoDreamer [Paliwal et al. 2024] and PanoDiffusion [Wu et al. 2023b] attempt to synthesize entire 360° panoramic images with depth information through in- or outpainting. Rather than iteratively expanding standard 2D images, other methods focus on creating 360° panorama images in a single step [Li et al. 2024; Stan et al. 2023; Tang et al. 2024; Zhou et al. 2024a]. Another area of research addresses the handling of occlusions via multi-view generation [Ye et al. 2024], layered approaches [Yang et al. 2024c] or explicitly defining the corresponding entities [Zhou et al. 2025]. Video diffusion models have strong temporal coherency but are still limited in generating 3D content that is consistent along long camera trajectories [Chen et al. 2025b; Ren et al. 2025; Yu et al. 2024c; Zhai et al. 2025; Zhang et al. 2025]. While image-based methods offer strong visual quality and global coherence, they generally lack fine-grained control over individual scene elements and are limited in navigational flexibility, especially when compared to compositional scene generation approaches, which we discuss in the following section.

### 2.2 Compositional Scene Generation

In contrast to monolithic approaches, compositional scene generation focuses on constructing scenes from multiple, independently generated objects which can be edited or animated. Recent advances

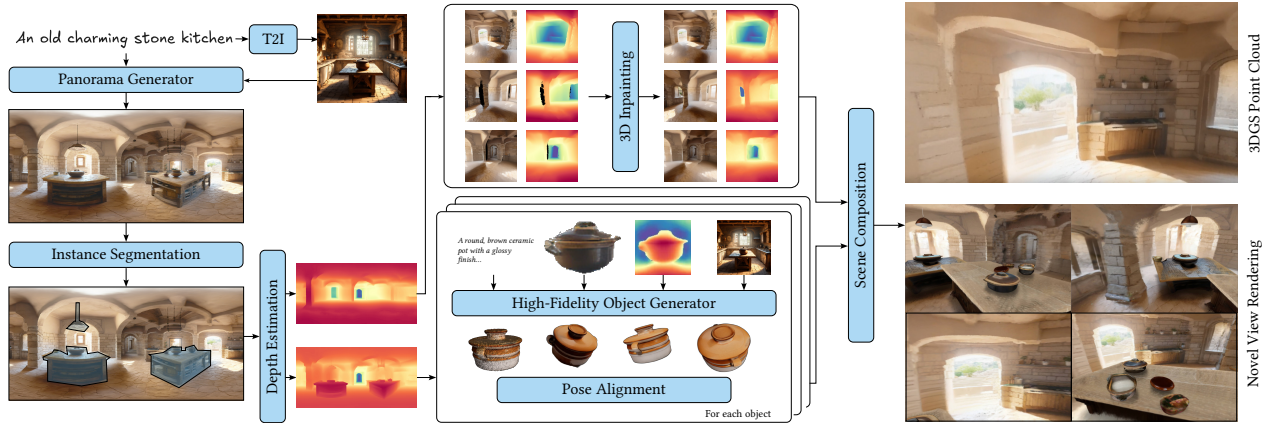


Fig. 2. An overview of our architecture. We start by generating a 360° panorama, followed by instance segmentation to separate the foreground objects from the scene background. Segmented objects are lifted to 3D using semantic and geometric priors, while a 3D inpainting process converts the image to a 3DGS representation and fills disoccluded regions. Finally, the scene is composited, enabling navigation of the 3D environment at interactive rates.

in this area predominantly leverage pre-trained image diffusion models for scene generation [Chen et al. 2025a; Dogaru et al. 2024; Han et al. 2024; Huang et al. 2024; Zhou et al. 2024b]. The key differences between these methods lie in the strategies used to layout the scene.

Image-guided methods [Dogaru et al. 2024; Han et al. 2024; Huang et al. 2024; Zhang et al. 2023c; Zhou et al. 2024b] use generated or real images to infer each object’s location and orientation in the scene. Similarly, distillation-based approaches [Chen et al. 2025a; Epstein et al. 2024; Li et al. 2025] employ diffusion models to guide object placement. However, since these methods typically rely on single (non-panoramic) images, they are often limited in terms of scale and global coherence of the generated scenes.

To overcome these limitations, proxy-guided techniques introduce explicit control over scene structure, for example by letting users define the scene structure through various semantic annotations or by placing proxy geometries [Cohen-Bar et al. 2023; Fang et al. 2023; Schult et al. 2024; Wu et al. 2024; Yang et al. 2024b]. While these techniques provide great flexibility in terms of scale and coherence, they typically require extensive user input and manual scene design.

Overall, compositional approaches provide a powerful alternative to image-based scene generation, trading off the ease of automation for improved control, reusability, and interpretability of individual scene elements.

### 3 METHOD

The DreamAnywhere architecture proceeds through three stages. In the **first stage**, a 360° panoramic image  $I_F$  is generated from a text prompt and stylized by an input perspective image. From  $I_F$ , foreground objects are identified, segmented, and erased, producing a *clean* background image  $I_B$ . Then, the depth of  $I_B$  is aligned to that of  $I_F$ , producing a single, unified depth map and laying the groundwork for subsequent 3D composition. The **second stage** focuses on generating high-fidelity 3D Gaussian Splatting (3DGS) models of the segmented objects and computing their transformations for accurate placement in the 3D scene. In parallel, the **third stage** converts

the background image  $I_B$  into a high-resolution 3DGS point cloud. During this process, disoccluded regions are inpainted to ensure visual consistency across viewpoints under novel camera offsets. Finally, the outputs of the second (objects) and third (background) stages are fused into a unified 3DGS scene, enabling immersive and interactive navigation. An overview of our pipeline is illustrated in Figure 2. The remainder of this section presents all the components of our system, emphasizing the most essential technical and implementation details. Additional information and extended ablation studies regarding 2D and 3D inpainting, object and background generation, pose estimation and scene compositing are available in the supplementary material.

#### 3.1 Image Generation

**3.1.1 360° Panorama Diffusion.** The initial stage of our pipeline generates the 360° panoramic image  $I_F$  from a user-provided text prompt. To improve generalization and style fidelity, we guide the generation process using a perspective image derived from the same prompt, providing soft conditioning without enforcing pixel-level alignment. Existing panoramic diffusion models are typically LoRA-fine-tuned on small, less-diverse equirectangular datasets, limiting their ability to generalize to out-of-distribution styles/compositions despite these capabilities existing in the pre-trained base model.

To address this, we condition the diffusion process of the 360° image with a perspective image derived from the same text prompt, using an IP-Adapter-style mechanism [Ye et al. 2023]. We observe that simply adding this mechanism post-hoc to a panoramic LoRA model is ineffective due to a mismatch in perspective (for IP-Adapter) and panoramic (for LoRA) training distributions as shown in the ablation in Figure 9. Instead, we *jointly* fine-tune the panoramic LoRA with the IP-adapter, enabling effective style transfer from perspective to panoramic images. We base our model on Stable-Diffusion-3.5-Large and fine-tune a rank-8 LoRA on top of all attention blocks on a mix of indoor [Chang et al. 2017] and outdoor [PolyHaven 2025]. We train the model for 10k iterations with a learning rate of  $10^{-5}$  and a batch size of 4.

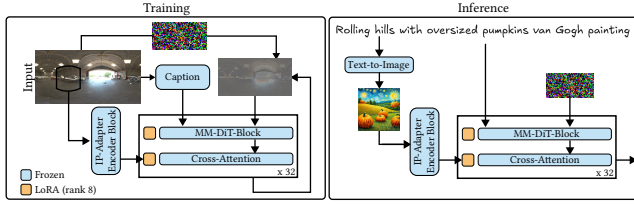


Fig. 3. Our image generation pipeline uses a diffusion model to denoise an equirectangular image [Feng et al. 2023; Yang et al. 2024c] but additionally combines perspective image conditioning through a decoupled cross-attention layer [Ye et al. 2023]. We train an equirectangular LoRA jointly with the perspective pre-trained cross attention layer, by encoding random perspective crops of the panorama, showing stronger generalization capabilities to out-of-domain panorama sampling.

**3.1.2 Instance Segmentation.** To identify suitable candidates for object reconstruction in the 360° images, we employ the off-the-shelf open-set segmentation pipeline *Grounded-SAM* [Ren et al. 2024]. To improve robustness in stylized or out-of-distribution scenes, we replace the original class identification stage (RAM [Zhang et al. 2023a]) with a larger vision-language model (GPT-4V), improving category recognition under diverse visual conditions. Given the limitations of current object generators, we exclude categories that are not good candidates for object reconstruction and are typically considered background elements (such as grass, walls, and floors). To further ensure high-quality segmentation, we sort all detected objects by their predicted IoU confidence and retain only the highest-scoring masks. For each retained object, the pipeline outputs a class identifier, a textual description, and a fine-grained segmentation mask, which are later used in Section 3.2.

**3.1.3 2D Inpainting.** We generate the background panorama  $I_B$  by erasing the foreground objects identified in the full panorama using the union of their segmentation masks. To synthesize plausible new content in the masked regions, we employ a diffusion-based inpainting model, Dreamshaper-8-Inpainting, [Lykon 2023], chosen for its ability to synthesize meaningful background content. We reduce hallucinations and artifacts in a two-stage process. First, we pre-inpaint the masked regions using LaMA [Suvorov et al. 2022] to obtain a coherent object-free initialization. Second we feed this through a custom LoRA fine-tuned on panoramic images from the Structured3D dataset [Zheng et al. 2020] for indoor defurnishing (in a similar spirit to [Slavcheva et al. 2024]). To further improve image quality, we apply standard techniques: the segmentation masks are slightly dilated, wrap-around consistency is enforced via horizontal padding (256 pixels), and Poisson blending seamlessly integrates the original panorama with the newly inpainted content. Although we experimented with repurposing the panoramic LoRA for inpainting, we found that a dedicated, specialized pipeline significantly reduces hallucinations without requiring manual intervention, especially in indoor scenes. The resulting empty panorama image is then lifted to 3D to form the background point cloud as described in Section 3.3.

**3.1.4 Depth Estimation.** We employ different depth estimation strategies for indoor and outdoor scenes due to their distinct geometric challenges. For indoor scenes, we use EGformer [Yun et al. 2023], which excels in predicting the axis-aligned structure typical of indoor environments. For outdoor scenes, we instead use the 360MonoDepth framework [Rey-Area et al. 2022], which aligns multiple perspective depth estimates obtained with Depth-Anything-V2 and possesses strong zero-shot generalization capabilities. To address unreliable depth predictions in low-detail regions, such as the sky, we explicitly detect and segment these areas using GroundedSAM [Ren et al. 2024] and assign the maximum depth value to ensure accurate representation. By construction, we obtain two independent depth estimates for  $I_F$  and  $I_B$  and perform an alignment step from  $I_B$  to  $I_F$  to ensure that objects are placed properly in their corresponding locations. Similarly to concurrent work, we find that a global affine transform is not sufficient and instead employ a per-pixel shift and global scale that minimizes the  $L_2$  depth error in overlapping regions between the images, subject to as-rigid-as-possible constraints [Sorkine and Alexa 2007].

### 3.2 High Quality Object Generation

To enable stylistically aligned and geometrically consistent 3D object reconstructions, we condition image-to-3D models using RGBD data derived from the segmented panorama. However, segmented object images are often incomplete, low-resolution, visible from suboptimal viewpoints, or contain generative artifacts (such as distortions or incorrect limbs). To overcome these problems, we introduce a resynthesis step that produces a high-quality reference image of the object, utilizing both semantic and geometric cues. This image is then used to guide the 3D reconstruction of each object. Our pipeline consists of three stages: reference image generation, 3D object generation, and pose estimation for accurate placement in the scene. We illustrate this process in Figure 4.

**3.2.1 Reference Image Generation.** We synthesize a high-resolution reference image for each object by conditioning a diffusion model on the available multimodal cues. First, we extract a textual description of the object by prompting a vision-language model with a perspective view of a crop containing the object. This includes a description of the object’s visual attributes such as pose and color, serving as the primary conditioning signal. Second, we compute a partial depth map by combining the object’s segmentation mask with the estimated depth, offering geometric guidance for shape. Finally, we include a style image, reused from the panorama generation process, to ensure visual consistency and thematic coherence across the scene. As shown in Figure 5, our approach results in realistic and style-consistent object views. This approach is better suited for downstream 3D reconstruction compared to other diffusion-based amodal completion methods (see Figure 6).

**3.2.2 Image-based Object Generation.** Our object reconstruction pipeline first generates six multi-view images at fixed camera poses, and then transforms them into a NeRF representation that captures both the geometry and color of the object. We found NeRF to be more robust than 3DGS as a differentiable representation when learning the reconstruction. Therefore, we opt to transform it into 3DGS

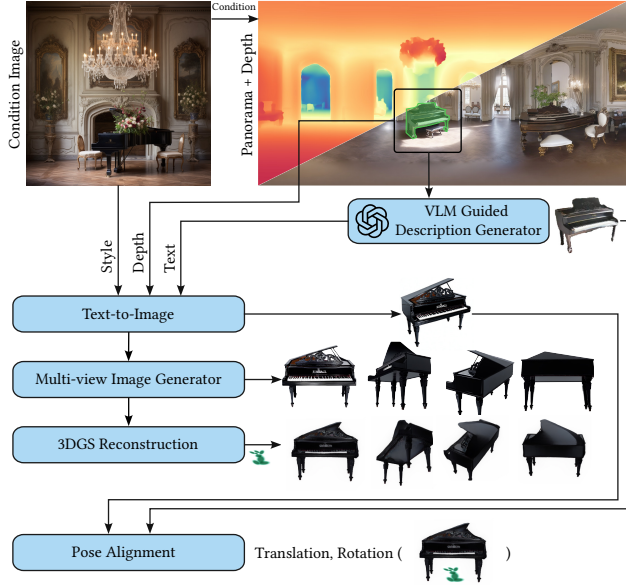


Fig. 4. Our object reconstruction pipeline leverages the panorama and style information to generate a high-resolution reference image to be used for multi-view generation. The generated multi-view images are then transformed into 3D Gaussian splats through a reconstruction pipeline. Finally, we align the generated object with the original and place it in the scene.

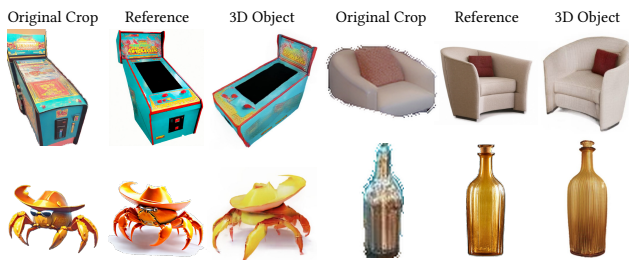


Fig. 5. Qualitative evaluation of our object reconstruction module. Employing multimodal cues faithfully captures the stylistic and structural essence of low-fidelity or incomplete objects, reconstructing a suitable 3D counterpart to be later placed in the environment.

in a separate post-processing step. We leverage Zero123++ [Shi et al. 2023] for the multi-view generation task and use the triplane decoder of InstantMesh [Xu et al. 2024] to convert the multi-view images into NeRF.

In practice, generative models often introduce artifacts, including transparency, incomplete regions or structural inconsistencies. To enable a reliable and automated object reconstruction pipeline, we introduce a single-round refinement stage after generation. During this stage, we generate multiple object candidates and rank them by visual quality and alignment with the original input image using a VLM, similar to [Zhou et al. 2025]. The VLM selects the best result from five candidates, one of which is generated using only the original cropped object image.



Fig. 6. Diffusion-based amodal completion methods (such as pix2gestalt [Ozguroglu et al. 2024] and Gen3DSR [Dogaru et al. 2024]) face challenges in producing high-quality inputs for multi-view image generation. Our method prioritizes structural fidelity by resynthesizing the reference image to yield higher quality 3D reconstructions.

**3.2.3 Pose Estimation.** We decompose object pose estimation into two parts: the absolute pose of the original object  $O_{\text{crop}}$  with respect to the viewing origin and the relative transformation between  $O_{\text{crop}}$  and its high-quality counterpart  $O_{\text{hq}}$ . The absolute pose is estimated by projecting the crop’s midpoint along a ray from the camera origin to the estimated mean depth. Orientation and scale are heuristically derived based on the crop geometry and panorama alignment. This provides a coarse but coherent placement aligned with the image-plane and panorama geometry. To semantically align the point cloud of the high-quality object  $O_{\text{hq}}$  with the original  $O_{\text{crop}}$  we compute the relative pose between them. We employ MAST3R [Leroy et al. 2024] on image pairs (perspective projections) of the original and high-quality object to obtain the relative pose. The final pose of  $O_{\text{hq}}$  preserves semantic alignment with the original object’s placement.

### 3.3 3D Background Generation

Generating a 3D scene suitable for exploration from a single 360° image is an underconstrained problem, as the available information is limited to a single viewpoint. To address this, we employ a three-step process that reconstructs missing scene content through a combination of inpainting and score distillation sampling (SDS) [Poole et al. 2023]. First, we optimally initialize the 3DGS point cloud from the panoramic image and prepare disocclusions for inpainting through a pretuning stage; Second, we incrementally populate disocclusions with new Gaussians through a 3D inpainting process conditioned on the existing point cloud; Finally, we ensure multi-view consistency by applying SDS on a larger set of possible views. During all optimization steps, we leverage MCMC-densification [Kheradmand et al. 2024], a process demonstrated in Figure 7.

**3.3.1 Background Initialization and Pretuning.** We initialize the 3DGS point cloud by unprojecting the pixels through a spherical camera placed at the origin, where the covariance matrices are initialized from normals derived from the depth map  $D_B$ , resulting in pixel-tight views when viewed from the origin. For pretuning, we optimize the initial Gaussians using mixed supervision from an upscaled version of the background panorama  $I_B$  (90%) and random views (10%). The  $I_B$  loss follows standard 3DGS supervision, while the random-view supervision focuses on identifying disoccluded regions.

**3.3.2 Incremental Inpainting.** To synthesize realistic new content in disoccluded regions, we leverage a pre-trained inpainting model

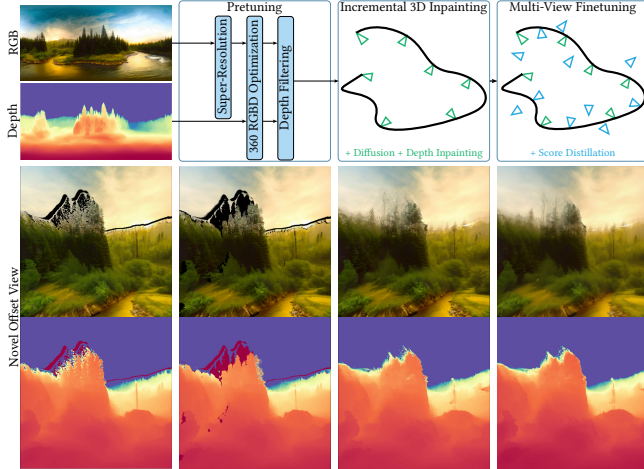


Fig. 7. The background generation stage starts by identifying large occluded regions and preparing the 3DGS point cloud for inpainting, then proceeds to incrementally fill in new content and finally enforces multi-view consistency when rendering from novel views with score distillation.

conditioned on the rendered projections of the existing 3DGS splats. Specifically, we select a set of keyframes that target important regions with missing content. For each keyframe we render the point cloud and generate an inpainted RGB image and an inpainting mask, computed by applying max-pooling (kernel size 25) and thresholding ( $T < 0.5$ ) on the transmittance map  $T$ , isolating low-opacity regions as targets for inpainting. For each pixel in the target region, we instantiate a new Gaussian by unprojecting it with a scene-aligned depth estimate. This depth is obtained using a diffusion model repurposed and fine-tuned for 3DGS depth inpainting [Liu et al. 2024], and provides a strong geometric prior. The inpainting process is done incrementally per keyframe, minimizing inconsistencies across overlapping views, similarly to [Höllein et al. 2023].

**3.3.3 Multi-view Fine-tuning.** Finally, to consolidate the inpainted views with the existing 3D content, we employ mixed supervision from the panorama image (25%), the inpainted images (25%) and SDS [Poole et al. 2023] from random views around the inpainted regions (50%). This final stage of SDS fine-tuning helps to remove view-inconsistencies and ensures that the Gaussians introduced during inpainting are consistent and aligned with the existing scene.

### 3.4 Composition

The last stage of the pipeline composes the final scene, by placing the 3D objects onto the background point cloud’s world frame, resulting in a navigable 3D scene. Since the scene consists of a set of splat parameters and their explicit transformations, post-processing effects and re-positioning of objects can be applied trivially, a key strength of the proposed system.

To further improve visual coherence, we address two key sources of error that can disrupt immersion. The first is the elimination of contact shadows — an unavoidable consequence of the mask dilation step used during object removal. Since achieving full control over lighting in diffusion models [Corvi et al. 2023; Guo et al. 2023] and

Table 1. Quantitative evaluation of our method against Text2Room [Höllein et al. 2023], DreamScene360 [Zhou et al. 2025] and Layerpano3D [Yang et al. 2024c]. Metrics are averaged across all scenes and computed on 136 frames per scene. Our method has state-of-the-art performance in terms of perceptual image quality and visual aesthetics. The differences in CLIP scores (evaluated against the original text prompt) are small and should be interpreted with care (see main text).

Method	CLIP↑	Q-ALIGN↑	A-ALIGN↑	CLIP-IQA+↑
Ours	20.565	<b>3.427</b>	<b>3.121</b>	<b>0.461</b>
Text2Room	<b>20.779</b>	2.998	<u>2.872</u>	0.432
DreamScene360	20.615	2.510	2.517	0.347
Layerpano3D	<u>20.721</u>	<u>3.383</u>	2.833	<u>0.421</u>

relighting remain challenging problems, we reintroduce shadows through a splat-aware shadow mapping pass (details in the supplemental). The second issue involves inaccurate pose estimation, which can lead to objects violating physical plausibility. To mitigate this, we automatically snap object positions to dominant support planes (e.g. floor or walls), ensuring a more realistic and physically grounded scene integration.

## 4 RESULTS

In this section we provide a quantitative and qualitative evaluation on the scene generation task, as well as an ablation of the core components of our pipeline. To assess the effectiveness of our approach in generating 3D scenes from text prompts, we focus on its ability to produce coherent and immersive scenes with high-quality and structurally consistent novel view synthesis. We compare our method against three state-of-the-art approaches for immersive scene generation: LayerPano3D [Yang et al. 2024c], Text2Room [Höllein et al. 2023], and DreamScene360 [Zhou et al. 2025]. Additionally, in Figure 8 we provide a qualitative comparison with other methods that share a similar goal but for which a direct comparison is non-trivial.

Our method is evaluated on 17 text prompts commonly found in recent literature [Shriram et al. 2024; Yang et al. 2024c]. For each scene we recorded a 6-second walk-through video (at  $1024 \times 1024$ px resolution) along a predefined camera trajectory *different* from the one used for the optimization described in Section 3.3, covering large parts of the scene’s geometry as well as occluded surfaces. Examples of video frames are shown in Figure 11.

We generated all scenes on a single NVIDIA H100, with each scene typically taking 10-15m to generate, given an average of 7.5 objects per scene. More results can be found in Figure 12.

### 4.1 Quantitative Evaluation

We quantitatively evaluate prompt alignment and image quality. To measure image quality and aesthetics, we use CLIP-IQA+ [Wang et al. 2023], Q-Align and A-Align [Wu et al. 2023a] metrics. To quantify prompt alignment we compute the CLIPScore [Hessel et al. 2021] between the prompt and each rendered frame. The results in Table 1 demonstrate that our method outperforms competing work in terms of both image quality and aesthetics metrics. For completeness, we also evaluate CLIP scores on single views against the scene’s text prompt. However, individual views typically capture



Fig. 8. Qualitative evaluation against WonderWorld [Yu et al. 2024a], DreamScene [Li et al. 2025] and ViewCrafter [Yu et al. 2024c]. WonderWorld degenerates into flat, view-dependent renderings when shown from out-of-context viewpoints, whereas DreamScene exhibits reduced fidelity in complex regions and object poses while expecting the positioning of objects to be known a priori. ViewCrafter combines video diffusion and reconstruction models but it is not able to maintain 3D coherence for long camera paths.



Fig. 9. Qualitative ablation of out-of-domain sampling for panorama generator models. Our method captures the stylistic guidance faithfully, but without IP-Adapter it reverts back to its base panoramic distribution similarly to other recent methods. Simply using a perspective IP-Adapter does not work because of the mismatching distributions at training time.

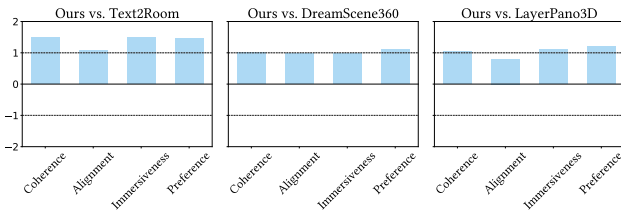


Fig. 10. User study results for pairwise comparisons between our method, DreamScene360, Text2Room and LayerPano3D. Ratings are given on a 5-point Likert scale capturing strong, weak and no preference between the approaches. The participants rated our approach higher than the comparison methods on all axes.

only a small portion of the scene, making CLIP scores a less reliable metric for our novel view evaluation.

## 4.2 Qualitative Evaluation

**4.2.1 Comparison.** Figure 11 provides a side-by-side comparison of the scenes generated by the different methods. In general, the results from Text2Room exhibit repetitive content and resemble stitched two-dimensional paintings—particularly in outdoor scenes—which limits the creation of immersive environments. However, the resulting images naturally excel in sharpness and detail, due to the method’s use of meshes for 3D representation. LayerPano3D and DreamScene360 demonstrate some capability for novel view synthesis, but struggle when scenes are viewed with significant offsets, such as sideways perspectives of objects.

**4.2.2 Ablation.** We present an ablation of the image generator architecture and the necessity for the joint fine-tuning procedure in Figure 9, comparing it to [Yang et al. 2024c] and [Zhang et al. 2024]. Despite training on only a subset of the public data used by [Yang et al. 2024c], we demonstrate stronger prompt adherence.

Our object generation module effectively addresses several common challenges in object extraction from images, such as panoramic distortion, low-resolution crops, and imperfect segmentation masks. Examples of these issues are illustrated in Figure 6. One alternative is to apply super-resolution and amodal completion but this approach typically requires multiple specialized modules, each with its own issues (Figure 5). Generating the same level of detail with super-resolution techniques on the panoramic image is still a challenge and requires much larger network architectures.

## 4.3 User Study

To assess the effectiveness of our model in generating immersive and navigable 3D scenes, we conducted a user study with 28 participants, including graduate students and professionals in graphics and vision. Participants evaluated short videos of scenes on: *Coherence*: Do the spatial layout, object placement, and interactions in the scene form a logical and believable whole?; *Compatibility*: Do the objects, materials, lighting, and textures align well with the given text prompt?; *Immersiveness*: Does the scene convincingly represent a 3D environment, evoking a sense of depth, realism and presence?; *Overall Preference*. Each comparison was rated from  $-2$  to  $+2$ . As shown in Table 1, our method was consistently preferred across all metrics and in particular was praised for its geometric structure in novel view synthesis, as shown by the *coherence* and *immersiveness* scores. The results were statistically significant ( $p < .001$ ) according to the Wilcoxon signed rank tests.

## 5 DISCUSSION AND LIMITATIONS

The modular nature of our pipeline has the disadvantage of having multiple possible points of failure. Conversely, this very modularity, serves as a significant advantage for targeted user intervention, which is often desired in generative applications. It also facilitates easy replacement of individual modules (e.g. the image generator method with [Yang et al. 2024c] or the 3D inpainting step with [Yu et al. 2024c]). A core strength of our method lies in its ability to generate globally coherent 3D scenes that remain consistent across a wide range of viewpoints. While this comes at the cost of localized sharpness compared to models optimized for narrow view paths, it enables free exploration without structural artifacts or semantic

collapse. In contrast, video diffusion-based approaches typically reconstruct scenes from a predefined camera trajectory, yielding sharper results along that path but failing to generalize beyond it. This makes direct comparisons inherently asymmetric. To provide a fairer assessment, we demonstrate in Figure 12 and the accompanying video how our method can optionally be combined with a video-to-video diffusion model (e.g., Cosmos-Transfer1 [Alhaja et al. 2025]) to enhance rendering sharpness along known view paths. This hybrid configuration showcases the flexibility of our modular pipeline and illustrates the upper bound of visual quality achievable with targeted post-processing, making our system competitive even in restricted-view settings.

## 6 CONCLUSION

This work presented DreamAnywhere, a novel framework for generating immersive 3D scenes from text prompts by leveraging 360° panoramic images as foundational priors. Its modular, object-centric pipeline separates background and object generation, enabling high-fidelity object reconstruction and coherent scene completion through hybrid inpainting techniques. Compared to existing methods, DreamAnywhere significantly enhances novel view synthesis coherence and offers robust performance for navigable 3D environments, as validated by quantitative results and strong user preference. This approach facilitates downstream applications like scene editing and simulation, paving the way for more scalable and interactive 3D content creation.

## REFERENCES

Hassan Abu Alhaja, Jose Alvarez, Maciej Bala, Tiffany Cai, Tianshi Cao, Liz Cha, Joshua Chen, Mike Chen, Francesco Ferroni, Sanja Fidler, et al. 2025. Cosmos-Transfer1: Conditional World Generation with Adaptive Multimodal Control. arXiv:2503.14492

Iro Armeni, Zhi-Yang He, JunYoung Gwak, Amir R Zamir, Martin Fischer, Jitendra Malik, and Silvio Savarese. 2019. 3D Scene Graph: A Structure for Unified Semantics, 3D Space, and Camera. In *Proceedings of the IEEE/CVF International Conference on Computer Vision (ICCV)*. 5663–5672. <https://doi.org/10.1109/ICCV.2019.00576>

Mathilde Caron, Hugo Touvron, Ishan Misra, Hervé Jégou, Julien Mairal, Piotr Bojanowski, and Armand Joulin. 2021. Emerging Properties in Self-Supervised Vision Transformers. In *Proceedings of the IEEE/CVF International Conference on Computer Vision (ICCV)*. <https://doi.org/10.1109/ICCV48922.2021.00951>

Angel Chang, Angela Dai, Thomas Funkhouser, Maciej Halber, Matthias Nießner, Manolis Savva, Shuran Song, Andy Zeng, and Yinda Zhang. 2017. Matterport3D: Learning from RGB-D Data in Indoor Environments. *Proceedings of the International Conference on 3D Vision (3DV)*, 667–676. <https://doi.org/10.1109/3DV.2017.00081>

Luxi Chen, Zihan Zhou, Min Zhao, Yikai Wang, Ge Zhang, Wenhao Huang, Hao Sun, Ji-Rong Wen, and Chongxuan Li. 2025b. FlexWorld: Progressively Expanding 3D Scenes for Flexible-View Synthesis. arXiv:2503.13265

Yongwei Chen, Tengfei Wang, Tong Wu, Xingang Pan, Kui Jia, and Ziwei Liu. 2025a. ComboVerse: Compositional 3D Assets Creation Using Spatially-Aware Diffusion Guidance. In *Proceedings of the European Conference on Computer Vision (ECCV)*. 128–146. [https://doi.org/10.1007/978-3-031-72691-0\\_8](https://doi.org/10.1007/978-3-031-72691-0_8)

Dana Cohen-Bar, Elad Richardson, Gal Metzer, Raja Giryes, and Daniel Cohen-Or. 2023. Set-the-Scene: Global-Local Training for Generating Controllable NeRF Scenes. In *Proceedings of the IEEE/CVF International Conference on Computer Vision (ICCV) Workshops*. 2920–2929. <https://doi.org/10.1109/ICCVW60793.2023.00314>

Riccardo Corvi, Davide Cozzolino, Giada Zingarini, Giovanni Poggi, Koki Nagano, and Luisa Verdoliva. 2023. On The Detection of Synthetic Images Generated by Diffusion Models. In *ICASSP 2023 IEEE International Conference on Acoustics, Speech and Signal Processing (ICASSP)*. 1–5. <https://doi.org/10.1109/ICASSP49357.2023.10095167>

Andrea Dogaru, Mert Özer, and Bernhard Egger. 2024. Generalizable 3D Scene Reconstruction via Divide and Conquer from a Single View. arXiv:2404.03421

Dave Epstein, Ben Poole, Ben Mildenhall, Alexei A. Efros, and Aleksander Holynski. 2024. Disentangled 3D Scene Generation with Layout Learning. In *Proceedings of the International Conference on Machine Learning (ICML)*. <https://doi.org/10.5555/3692070.3692570>

Chuan Fang, Xiaotao Hu, Kunming Luo, and Ping Tan. 2023. Ctrl-Room: Controllable Text-to-3D Room Meshes Generation with Layout Constraints. arXiv:2310.03602

Mengyang Feng, Jinlin Liu, Miaomiao Cui, and Xuansong Xie. 2023. Diffusion360: Seamless 360 Degree Panoramic Image Generation Based on Diffusion Models. arXiv:2311.13141

Rafail Fridman, Amit Abecasis, Yoni Kasten, and Tali Dekel. 2024. SceneScape: Text-Driven Consistent Scene Generation. In *Proceedings of the Conference on Neural Information Processing Systems (NeurIPS)*. Article 1734, 18 pages. <https://doi.org/10.5555/3666122.3667856>

Ming Gui, Johannes Schusterbauer, Ulrich Prestel, Pingchuan Ma, Dmytro Kotovenko, Olga Grebenkova, Stefan Andreas Baumann, Vincent Tao Hu, and Björn Ommer. 2024. DepthFM: Fast Monocular Depth Estimation with Flow Matching. arXiv:2403.13788

Langqing Guo, Chong Wang, Wenhan Yang, Siyu Huang, Yufei Wang, Hanspeter Pfister, and Bihan Wen. 2023. Shadowdiffusion: When Degradation Prior Meets Diffusion Model for Shadow Removal. In *Proceedings of the IEEE/CVF Conference on Computer Vision and Pattern Recognition (CVPR)*. 14049–14058. <https://doi.org/10.1109/CVPR52729.2023.01350>

Haonan Han, Rui Yang, Huan Liao, Jiankai Xing, Zunnan Xu, Xiaoming Yu, Junwei Zha, Xiu Li, and Wanhua Li. 2024. REPARO: Compositional 3D Assets Generation with Differentiable 3D Layout Alignment. arXiv:2405.18525

Jack Hessel, Ari Holtzman, Maxwell Forbes, Ronan Le Bras, and Yejin Choi. 2021. CLIP-Score: A Reference-free Evaluation Metric for Image Captioning. arXiv:2104.08718

Lukas Höllein, Ang Cao, Andrew Owens, Justin Johnson, and Matthias Nießner. 2023. Text2Room: Extracting Textured 3D Meshes from 2D Text-to-Image Models. In *Proceedings of the IEEE/CVF International Conference on Computer Vision (ICCV)*. 7909–7920. <https://doi.org/10.1109/ICCV51070.2023.00727>

Zehuan Huang, Yuanchen Guo, Xingqiao An, Yunhan Yang, Yangguang Li, Zixin Zou, Ding Liang, Xihui Liu, Yanpei Cao, and Lu Sheng. 2024. MIDI: Multi-Instance Diffusion for Single Image to 3D Scene Generation. arXiv:2412.03558

Bernhard Kerbl, Georgios Kopanas, Thomas Leimkühler, and George Drettakis. 2023. 3D Gaussian Splatting for Real-Time Radiance Field Rendering. *ACM Transactions on Graphics* 42, 4, Article 139 (2023), 14 pages. <https://doi.org/10.1145/3592433>

Bernhard Kerbl, Andreas Meuleman, Georgios Kopanas, Michael Wimmer, Alexandre Lanvin, and George Drettakis. 2024. A Hierarchical 3D Gaussian Representation for Real-Time Rendering of Very Large Datasets. *ACM Transactions on Graphics* 43, 4 (July 2024). <https://repo-sam.inria.fr/fungraph/hierarchical-3d-gaussians/>

Shakiba Kheradmand, Daniel Rebain, Gopal Sharma, Weiwei Sun, Yang-Che Tseng, Hossam Isack, Abhishek Kar, Andrea Tagliasacchi, and Kwang Moo Yi. 2024. 3D Gaussian Splatting as Markov Chain Monte Carlo. In *Proceedings of the Conference on Neural Information Processing Systems (NeurIPS)*. <https://openreview.net/pdf?id=UCSt4gk6iX>

Vincent Leroy, Johann Cabon, and Jerome Revaud. 2024. Grounding Image Matching in 3D with MAST3R. In *Proceedings of the European Conference on Computer Vision (ECCV)*. [https://doi.org/10.1007/978-3-031-73220-1\\_5](https://doi.org/10.1007/978-3-031-73220-1_5)

Chenghao Li, Chaoning Zhang, Joseph Cho, Atish Waghvase, Lik-Hang Lee, Francois Rameau, Yang Yang, Sung-Ho Bae, and Choong Seon Hong. 2023. Generative AI Meets 3D: A Survey on Text-to-3D in AIGC Era. arXiv:2305.06131

Haoran Li, Haolin Shi, Wenli Zhang, Wenjun Wu, Yong Liao, Lin Wang, Lik-Hang Lee, and Peng Yuan Zhou. 2025. DreamScene: 3D Gaussian-Based Text-to-3D Scene Generation via Formation Pattern Sampling. In *Proceedings of the European Conference on Computer Vision (ECCV)*. 214–230. [https://doi.org/10.1007/978-3-031-72904-1\\_13](https://doi.org/10.1007/978-3-031-72904-1_13)

Wenrui Li, Yapeng Mi, Fucheng Cai, Zhe Yang, Wangmeng Zuo, Xingtao Wang, and Xiaopeng Fan. 2024. SceneDreamer360: Text-Driven 3D-Consistent Scene Generation with Panoramic Gaussian Splatting. arXiv:2408.13711

Yixun Liang, Xin Yang, Jiantao Lin, Haodong Li, Xiaogang Xu, and Yingcong Chen. 2024. LucidDreamer: Towards High-Fidelity Text-to-3D Generation via Interval Score Matching. In *Proceedings of the IEEE/CVF Conference on Computer Vision and Pattern Recognition (CVPR)*. 6517–6526. <https://doi.org/10.1109/CVPR52733.2024.00623>

Andrew Liu, Richard Tucker, Varun Jampani, Ameesh Makadia, Noah Snavely, and Angjoo Kanazawa. 2021. Infinite Nature: Perpetual View Generation of Natural Scenes from a Single Image. In *Proceedings of the IEEE/CVF International Conference on Computer Vision (ICCV)*. <https://doi.org/10.1109/ICCV48922.2021.01419>

Zhiheng Liu, Hao Ouyang, Qiuyu Wang, Ka Leong Cheng, Jie Xiao, Kai Zhu, Nan Xue, Yu Liu, Yujun Shen, and Yang Cao. 2024. Infusion: Inpainting 3D Gaussians via Learning Depth Completion from Diffusion Prior. arXiv:2404.11613

Lyonk. 2023. DreamShaper v8 Inpainting. <https://huggingface.co/Lyonk/dreamshaper-8-inpainting>

Saswat Subhrajyoti Mallick, Rahul Goel, Bernhard Kerbl, Markus Steinberger, Francisco Vicente Carrasco, and Fernando De La Torre. 2024. Taming 3DGS: High-Quality Radiance Fields with Limited Resources. In *SIGGRAPH Asia 2024 Conference Papers (SA '24)*. Association for Computing Machinery, New York, NY, USA, Article 2, 11 pages. <https://doi.org/10.1145/3680528.3687694>

Ege Ozguroglu, Ruoshi Liu, Didac Surís, Dian Chen, Achal Dave, Pavel Tokmakov, and Carl Vondrick. 2024. pix2gestalt: Amodal Segmentation by Synthesizing Wholes. *Proceedings of the IEEE/CVF Conference on Computer Vision and Pattern Recognition (CVPR)* (2024), 3931–3940. <https://doi.org/10.1109/CVPR52733.2024.00377>

- Avinash Paliwal, Xilong Zhou, Andrii Tsarov, and Nima Khademi Kalantari. 2024. PanoDreamer: 3D Panorama Synthesis from a Single Image. arXiv:2412.04827
- Ryan Po, Wang Yifan, Vladislav Golyanik, Kfir Aberman, Jonathan T Barron, Amit Bermato, Eric Chan, Tali Dekel, Aleksander Holynski, Angjoo Kanazawa, et al. 2024. State of the Art on Diffusion Models for Visual Computing. *Computer Graphics Forum* 43, 2 (2024), e15063. <https://doi.org/10.1111/cgf.15063>
- PolyHaven. 2025. *PolyHaven*. <https://polyhaven.com/hdris>
- Ben Poole, Ajay Jain, Jonathan T. Barron, and Ben Mildenhall. 2023. DreamFusion: Text-to-3D using 2D Diffusion. In *Proceedings of the International Conference on Learning Representations (ICLR)*. <https://openreview.net/forum?id=FjNys5c7VyY>
- Tianhe Ren, Shilong Liu, Ailing Zeng, Jing Lin, Kunchang Li, He Cao, Jiayu Chen, Xinyu Huang, Yukang Chen, Feng Yan, Zhaoyang Zeng, Hao Zhang, Feng Li, Jie Yang, Hongyang Li, Qing Jiang, and Lei Zhang. 2024. Grounded SAM: Assembling Open-World Models for Diverse Visual Tasks. arXiv:2401.14159 <https://arxiv.org/abs/2401.14159>
- Xuanchi Ren, Tianchang Shen, Jiahui Huang, Huan Ling, Yifan Lu, Merlin Nimier-David, Thomas Müller, Alexander Keller, Sanja Fidler, and Jun Gao. 2025. GEN3C: 3D-Informed World-Consistent Video Generation with Precise Camera Control. arXiv:2503.03751
- Manuel Rey-Area, Mingze Yuan, and Christian Richardt. 2022. 360MonoDepth: High-Resolution 360° Monocular Depth Estimation. In *Proceedings of the IEEE/CVF Conference on Computer Vision and Pattern Recognition (CVPR)*. 3752–3762. <https://doi.org/10.1109/CVPR52688.2022.00374>
- Jonas Schult, Sam Tsai, Lukas Höllein, Bichen Wu, Jialiang Wang, Chih-Yao Ma, Kunpeng Li, Xiaofang Wang, Felix Wimbauer, Zijian He, Peizhao Zhang, Bastian Leibe, Peter Vajda, and Ji Hou. 2024. ControlRoom3D: Room Generation using Semantic Proxy Rooms. In *Proceedings of the IEEE/CVF Conference on Computer Vision and Pattern Recognition (CVPR)*. 6201–6210. <https://doi.org/10.1109/CVPR52733.2024.00593>
- Ruoxi Shi, Hansheng Chen, Zhuoyang Zhang, Minghua Liu, Chao Xu, Xinyue Wei, Linghao Chen, Chong Zeng, and Hao Su. 2023. Zero123++: a Single Image to Consistent Multi-view Diffusion Base Model. arXiv:2310.15110
- Jaidev Shriram, Alex Trevithick, Lingjie Liu, and Ravi Ramamoorthi. 2024. Realm-Dreamer: Text-Driven 3D Scene Generation with Inpainting and Depth Diffusion. arXiv:2404.07199
- Mira Slavcheva, Dave Gausebeck, Kevin Chen, David Buchhofer, Azwad Sabik, Chen Ma, Sachal Dhillon, Olaf Brandt, and Alan Dolhasz. 2024. An Empty Room is All We Want: Automatic Defurnishing of Indoor Panoramas. In *Proceedings of the IEEE/CVF Conference on Computer Vision and Pattern Recognition Workshops (CVPRW)*. 7384–7394. <https://doi.org/10.1109/CVPRW63382.2024.00734>
- Olga Sorkine and Marc Alexa. 2007. As-Rigid-As-Possible Surface Modeling. In *Proceedings of EUROGRAPHICS/ACM SIGGRAPH Symposium on Geometry Processing*. 109–116. <https://doi.org/10.5555/1281991.1282006>
- Gabriela Ben Melech Stan, Diana Wofk, Estelle Afllao, Shao-Yen Tseng, Zhipeng Cai, Michael Paulitsch, and Vasudev Lal. 2023. LDM3D-VR: Latent Diffusion Model for 3D VR. arXiv:2311.03226
- Roman Suvorov, Elizaveta Logacheva, Anton Mashikhin, Anastasia Remizova, Arsenii Ashukha, Aleksei Silvestrov, Naejin Kong, Harshith Goka, Kiwoong Park, and Victor Lempitsky. 2022. Resolution-robust Large Mask Inpainting with Fourier Convolutions. In *Proceedings of the IEEE/CVF Winter Conference on Applications of Computer Vision (WACV)*. 3172–3182. <https://doi.org/10.1109/WACV51458.2022.00323>
- Shitao Tang, Fuyang Zhang, Jiacheng Chen, Peng Wang, and Yasutaka Furukawa. 2024. MVDiffusion: Enabling Holistic Multi-view Image Generation with Correspondence-Aware Diffusion. In *Proceedings of the Conference on Neural Information Processing Systems (NeurIPS)*. Article 2229, 32 pages. <https://openreview.net/pdf?id=vA0vj1mY77>
- Xiang Tang, Ruotong Li, and Xiaopeng Fan. 2025. Recent Advance in 3D Object and Scene Generation: A Survey. arXiv:2504.11734
- Shubham Tulsiani, Saurabh Gupta, David Fouhey, Alexei A. Efros, and Jitendra Malik. 2018. Factoring Shape, Pose, and Layout from the 2D Image of a 3D Scene. In *Proceedings of the IEEE/CVF Conference on Computer Vision and Pattern Recognition (CVPR)*. 302–310. <https://doi.org/10.1109/CVPR.2018.00039>
- Jianyi Wang, Kelvin CK Chan, and Chen Change Loy. 2023. Exploring CLIP for Assessing the Look and Feel of Images. In *AAAI*. Article 284, 9 pages. <https://doi.org/10.1609/aaai.v37i2.25353>
- Xintao Wang, Liangbin Xie, Chao Dong, and Ying Shan. 2021. Real-ESRGAN: Training Real-World Blind Super-Resolution with Pure Synthetic Data. In *Proceedings of the IEEE/CVF International Conference on Computer Vision (ICCV) Workshops*. <https://doi.org/10.1109/ICCVW54120.2021.00217>
- Haoning Wu, Zicheng Zhang, Weixia Zhang, Chaofeng Chen, Chunyi Li, Liang Liao, Annan Wang, Erli Zhang, Wenxiu Sun, Qiong Yan, Xiongkuo Min, Guangtai Zhai, and Weisi Lin. 2023a. Q-Align: Teaching LLMs for Visual Scoring via Discrete Text-Defined Levels. arXiv:2312.17090
- Tianhao Wu, Chuanxia Zheng, and Tat-Jen Cham. 2023b. PanoDiffusion: 360-degree Panorama Outpainting via Diffusion. In *Proceedings of the International Conference on Learning Representations (ICLR)*. <https://openreview.net/forum?id=ZnZDXDFZOB>
- Zhennan Wu, Yang Li, Han Yan, Taizhang Shang, Weixuan Sun, Senbo Wang, Ruikai Cui, Weizhe Liu, Hiroyuki Sato, Hongdong Li, and Pan Ji. 2024. BlockFusion: Expandable 3D Scene Generation using Latent Tri-plane Extrapolation. *ACM Transactions on Graphics* 43, 4 (2024). <https://doi.org/10.1145/3658188>
- Jiale Xu, Weihao Cheng, Yiming Gao, Xintao Wang, Shenghua Gao, and Ying Shan. 2024. InstantMesh: Efficient 3D Mesh Generation from a Single Image with Sparse-view Large Reconstruction Models. arXiv:2404.07191
- Lihe Yang, Bingyi Kang, Zilong Huang, Zhen Zhao, Xiaogang Xu, Jiashi Feng, and Hengshuang Zhao. 2024a. Depth Anything V2. In *Proceedings of the Conference on Neural Information Processing Systems (NeurIPS)*. <https://openreview.net/forum?id=cFTi3gLJ1X>
- Shuai Yang, Jing Tan, Mengchen Zhang, Tong Wu, Yixuan Li, Gordon Wetzstein, Ziwei Liu, and Dahua Lin. 2024c. LayerPano3D: Layered 3D Panorama for Hyper-Immersive Scene Generation. (2024). arXiv:2408.13252
- Tao Yang, Rongyuan Wu, Peiran Ren, Xuansong Xie, and Lei Zhang. 2023. Pixel-Aware Stable Diffusion for Realistic Image Super-Resolution and Personalized Stylization. In *Proceedings of the European Conference on Computer Vision (ECCV)*. [https://doi.org/10.1007/978-3-031-73247-8\\_5](https://doi.org/10.1007/978-3-031-73247-8_5)
- Xiuyu Yang, Yunze Man, Jun-Kun Chen, and Yu-Xiong Wang. 2024b. SceneCraft: Layout-Guided 3D Scene Generation. In *Proceedings of the Conference on Neural Information Processing Systems (NeurIPS)*. <https://openreview.net/pdf?id=CTvnxAcSJN>
- Hu Ye, Jun Zhang, Sibao Liu, Xiao Han, and Wei Yang. 2023. IP-Adapter: Text Compatible Image Prompt Adapter for Text-to-Image Diffusion Models. arXiv:2308.06721
- Weicai Ye, Chenhao Ji, Zheng Chen, Junyao Gao, Xiaoshui Huang, Song-Hai Zhang, Wanli Ouyang, Tong He, Cairong Zhao, and Guofeng Zhang. 2024. DiffPano: Scalable and Consistent Text to Panorama Generation with Spherical Epipolar-Aware Diffusion. In *Proceedings of the Conference on Neural Information Processing Systems (NeurIPS)*. <https://openreview.net/forum?id=YOvVR40h5o>
- Hong-Xing Yu, Haoyi Duan, Charles Herrmann, William T. Freeman, and Jiajun Wu. 2024a. WonderWorld: Interactive 3D Scene Generation from a Single Image. arXiv:2406.09394
- Hong-Xing Yu, Haoyi Duan, Junhua Hur, Kyle Sargent, Michael Rubinstein, William T. Freeman, Forrester Cole, Deqing Sun, Noah Snively, Jiajun Wu, and Charles Herrmann. 2024b. WonderJourney: Going from Anywhere to Everywhere. In *Proceedings of the IEEE/CVF Conference on Computer Vision and Pattern Recognition (CVPR)*. <https://doi.org/10.1109/CVPR52733.2024.00636>
- Wangbo Yu, Jinbo Xing, Li Yuan, Wenbo Hu, Xiaoyu Li, Zhipeng Huang, Xiangjun Gao, Tien-Tsing Wong, Ying Shan, and Yonghong Tian. 2024c. ViewCrafter: Taming Video Diffusion Models for High-fidelity Novel View Synthesis. arXiv:2409.02048
- Ilwi Yun, Chanyong Shin, Hyunku Lee, Hyuk-Jae Lee, and Chae Eun Rhee. 2023. EGformer: Equirectangular Geometry-biased Transformer for 360 Depth Estimation. In *Proceedings of the IEEE/CVF International Conference on Computer Vision (ICCV)*. 6078–6089. <https://doi.org/10.1109/ICCV51070.2023.00561>
- Shangjin Zhai, Zhichao Ye, Jialin Liu, Weijian Xie, Jiaqi Hu, Zhen Peng, Hua Xue, Danpeng Chen, Xiaomeng Wang, Lei Yang, Nan Wang, Haomin Liu, and Guofeng Zhang. 2025. StarGen: A Spatiotemporal Autoregression Framework with Video Diffusion Model for Scalable and Controllable Scene Generation. arXiv:2501.05763
- Cheng Zhang, Qianyi Wu, Camilo Cruz Gambardella, Xiaoshui Huang, Dinh Phung, Wanli Ouyang, and Jianfei Cai. 2024. Taming Stable Diffusion for Text to 360° Panorama Image Generation. In *Proceedings of the IEEE/CVF Conference on Computer Vision and Pattern Recognition (CVPR)*. <https://doi.org/10.1109/CVPR52733.2024.00607>
- Jingbo Zhang, Xiaoyu Li, Ziyu Wan, Can Wang, and Jing Liao. 2023b. Text2NeRF: Text-Driven 3D Scene Generation With Neural Radiance Fields. *IEEE Transactions on Visualization and Computer Graphics* 30 (2023), 7749–7762. <https://api.semanticscholar.org/CorpusID:258822803>
- Qihang Zhang, Chaoyang Wang, Aliaksandr Siarohin, Peiye Zhuang, Yinghao Xu, Ceyuan Yang, Dahua Lin, Bo Dai, Bolei Zhou, Sergey Tulyakov, and Hsin-Ying Lee. 2023c. SceneWiz3D: Towards Text-guided 3D Scene Composition. In *Proceedings of the IEEE/CVF Conference on Computer Vision and Pattern Recognition (CVPR)*. <https://openreview.net/pdf?id=a5C3jms4S5>
- Shengjun Zhang, Jinzhao Li, Xin Fei, Hao Liu, and Yueqi Duan. 2025. Scene Splatter: Momentum 3D Scene Generation from Single Image with Video Diffusion Model. *IEEE / CVF Computer Vision and Pattern Recognition Conference (CVPR)* (2025). <https://doi.org/10.48550/arXiv.2504.02764>
- Youcai Zhang, Xinyu Huang, Jinyu Ma, Zhaoyang Li, Zhaochuan Luo, Yanchun Xie, Yuzhuo Qin, Tong Luo, Yaqian Li, Shilong Liu, et al. 2023a. Recognize Anything: A Strong Image Tagging Model. arXiv:2306.03514
- Jia Zheng, Junfei Zhang, Jing Li, Rui Tang, Shenghua Gao, and Zihan Zhou. 2020. Structured3D: A Large Photo-realistic Dataset for Structured 3D Modeling. In *Proceedings of The European Conference on Computer Vision (ECCV)*. [https://doi.org/10.1007/978-3-030-58545-7\\_30](https://doi.org/10.1007/978-3-030-58545-7_30)
- Haiyang Zhou, Xinhua Cheng, Wangbo Yu, Yonghong Tian, and Li Yuan. 2024a. HoloDreamer: Holistic 3D Panoramic World Generation from Text Descriptions. arXiv:2407.15187

Junsheng Zhou, Yu-Shen Liu, and Zhizhong Han. 2024b. Zero-Shot Scene Reconstruction from Single Images with Deep Prior Assembly. In *Proceedings of the Conference on Neural Information Processing Systems (NeurIPS)*. <https://openreview.net/pdf?id=SoTK84ewb7>

Shijie Zhou, Zhiwen Fan, Dejie Xu, Haoran Chang, Pradyumna Chari, Tejas Bharadwaj, Suya You, Zhangyang Wang, and Achuta Kadambi. 2025. DreamScene360: Unconstrained Text-to-3D Scene Generation with Panoramic Gaussian Splatting. In *Proceedings of the European Conference on Computer Vision (ECCV)*. 324–342. [https://doi.org/10.1007/978-3-031-72658-3\\_19](https://doi.org/10.1007/978-3-031-72658-3_19)

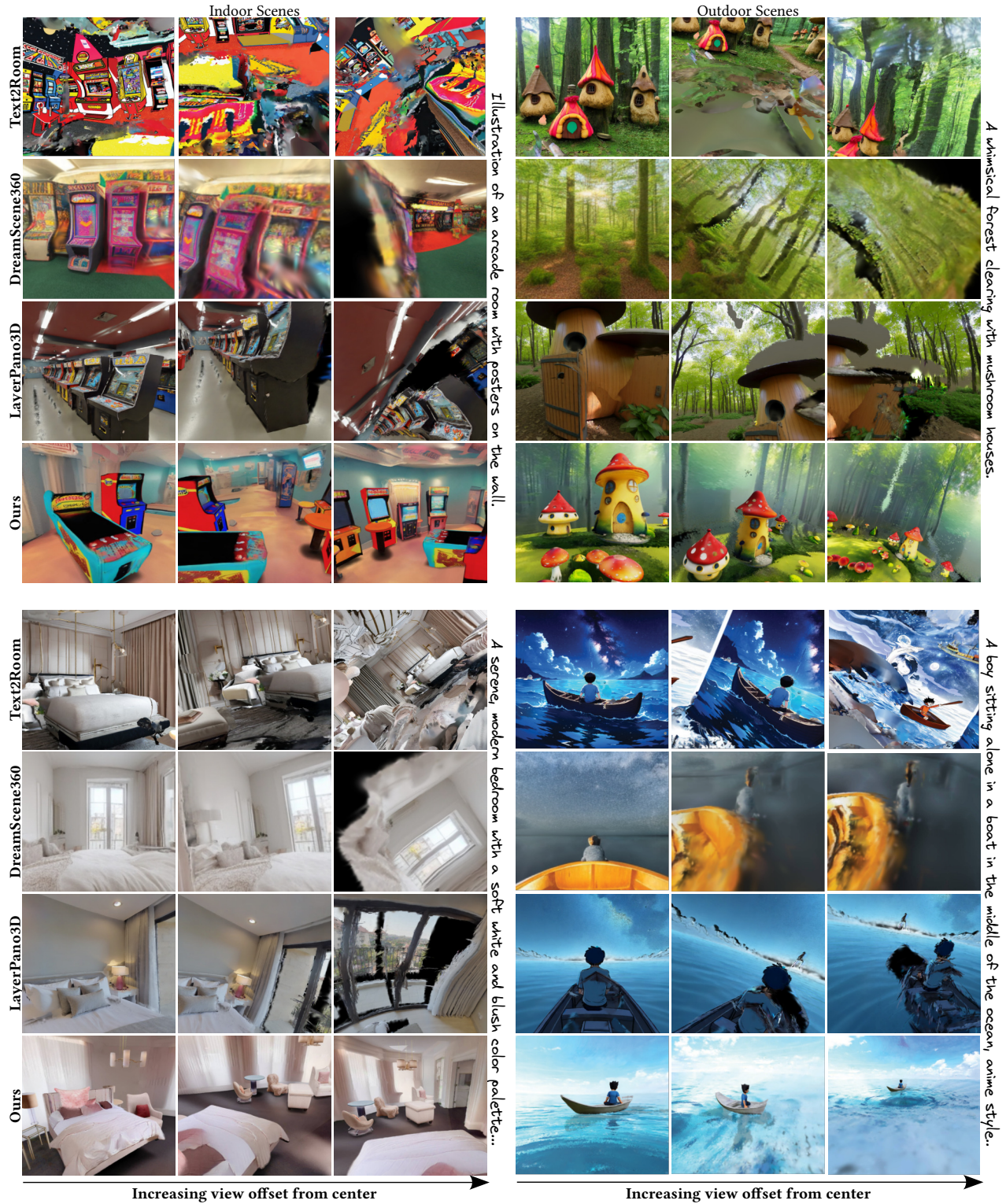


Fig. 11. Qualitative comparison with Text2Room [Höllein et al. 2023], DreamScene360 [Zhou et al. 2025] and LayerPano3D [Yang et al. 2024c]. Whereas scenes from these competing method suffer from disturbing artifacts for significant viewpoint changes, our method achieves coherent novel view synthesis for virtually all viewpoints.

Novel View Renderings

Cosmos-Transfer1



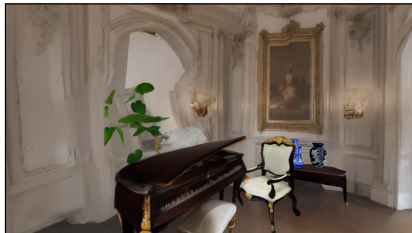
A lighthouse in the Arctic, van Gogh painting



A whimsical forest clearing with mushroom houses



A galactic saloon with an octopus serving drinks



A grand piano sits in a spacious room... painting and vases... chairs...



Rolling hills with oversized pumpkins and colorful flower fields, vibrant sky



A majestic peacock surfing a tall wave

Fig. 12. Additional results generated with our method across different indoor and outdoor environments. We show renderings from novel viewpoints unseen at training times as well as the result using Cosmos-Transfer1 [Alhajja et al. 2025], which can be used to increase sharpness as a post processing step, or if preferred viewing positions are known.

“The arcade machine is teal with vibrant yellow and red artwork. It’s rectangular, slanted back, and made of metal and plastic. Visible text includes: “Emperor” and “Anandapurs”. There are buttons and a coin slot. The arcade machine appears whole.”

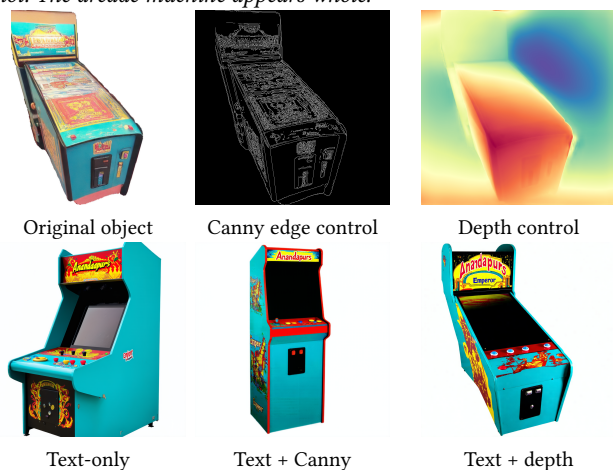


Fig. 13. Using Stable Diffusion in combination with a ControlNet gives object images that are much closer to the original object in comparison to images generated based on only the text description. From the original image we extract the Canny edge and depth control images. All re-generated images are generated using the text prompt shown at the top. From left to right we have the the image generated without additional conditioning, generated with additional Canny edge conditioning and generated with additional depth conditioning.

## A APPENDIX

### B 2D INPAINTING ABLATION

In Figure 14 we ablate the components to our 2D inpainting pipeline. Our complete approach that includes LaMA pre-inpainting and a fine-tuned LoRA leads to better results than what can be achieved with off-the-shelf Stable Diffusion inpainting. LaMa inpainting alone is not enough since the inpainted regions are still blurry. Our approach reduces the introduction of new objects in the inpainting regions when compared to Stable Diffusion inpainting.

### C OBJECT GENERATION DETAILS

To improve the similarity between objects as they occur in the original panorama image and the high-fidelity regenerated object, we employ depth and style conditioning in the text-to-image process. Figure 13 gives an overview of the effect that different conditioning signals have on the object generation process. Although unconstrained diffusion models might offer greater creative freedom, conditioning the new image on depth serves a dual purpose: not only does it preserve the object’s structural fidelity, it also enhances the robustness of the subsequent pose estimation between the original and newly obtained image. This approach proved to be more effective than conditioning on text-only. We also experimented with Canny edge control, but found it to be problematic, especially in case of partial objects for which it is incapable of completing the object.

### C.1 Implementation Details

For the object generation step we use the *large* version of the TEN-CENTARC/INSTANTMESH model with a render resolution of 512, 75 diffusion steps and a point cloud resolution of 128<sup>3</sup>. We generate 144 views uniformly distributed across a unit sphere (12 azimuth  $\times$  12 elevation angles) and generate color images from the triplane, while depth maps are extracted using the DEPTH-ANYTHING-V2 [Yang et al. 2024a] model. We train 3DGS with depth regularization enabled, following the methodology of Kerbl et al. [2023, 2024], for 5000 iterations. Although 1000 iterations typically suffice for good-quality object reconstruction, the extended training ensures optimal results. On average, a high-quality object is typically comprised of 30-50k Gaussians.

As depth-based ControlNet for the high-quality objects we use STABILITYAI/STABLE-DIFFUSION-3.5-LARGE-CONTROLNET-DEPTH in combination with STABILITYAI/STABLE-DIFFUSION-3.5-LARGE and a separate cross-attention layer for style conditioning [Ye et al. 2023]. We empirically set the control strength to 0.8 (depth) and 0.3 (style), a guidance scale of 7.5 and 50 inference steps. As a negative prompt we include “low quality, low resolution, blurry”. The depth control image is generated using DepthFM [Gui et al. 2024] after padding the crop image to a square size.

### C.2 NeRF to 3DGS conversion

To translate the triplane representation to 3DGS, we begin by generating a point cloud that identifies likely surface points in the volumetric representation using a regular grid. For each sample point, we compute density values through triplane sampling. Surface points are then identified using neighbor-based thresholding, guided by an empirically determined threshold of 0.2. These surface points are added as Gaussian locations in the point cloud, with their initial color values derived directly from the triplane representation. Next, we render 144 RGB-D images from positions uniformly distributed across a sphere. This spherical distribution ensures comprehensive coverage of the object’s geometry while providing robust supervision signals for reconstruction for standard 3DGS optimization with depth supervision [Kerbl et al. 2023, 2024]. Notably, this extraction process is significantly more efficient and robust than using COLMAP for point initialization.

## D POSE ESTIMATION AND SCENE ALIGNMENT DETAILS

*Reference Pose Estimation.* To estimate the reference pose of the original object  $O_{\text{crop}}$ , we utilize the crop mask to determine the mean depth  $d_m$  and the midpoint of the crop  $c_p$ . Considering the spherical model used for the panorama, with the camera placed at the origin, we move the object’s origin along a ray through  $c_p$  to depth  $d_m$ . By default, our object generation stage orients the object’s front-face along the Z-axis to match the 2D image input, *i.e.*, the image-plane of the 2D crop is fixed at the  $x/y$  plane in object-space. To ensure that the front face of the object is aligned towards the camera, we simply rotate the object around the vertical axis. To estimate the object’s scale, we unproject the crop’s corner points at depth  $d_m$  into world-space, treating the crop as the  $x/y$  front-face of the object’s bounding box. Finally, we apply a grounding

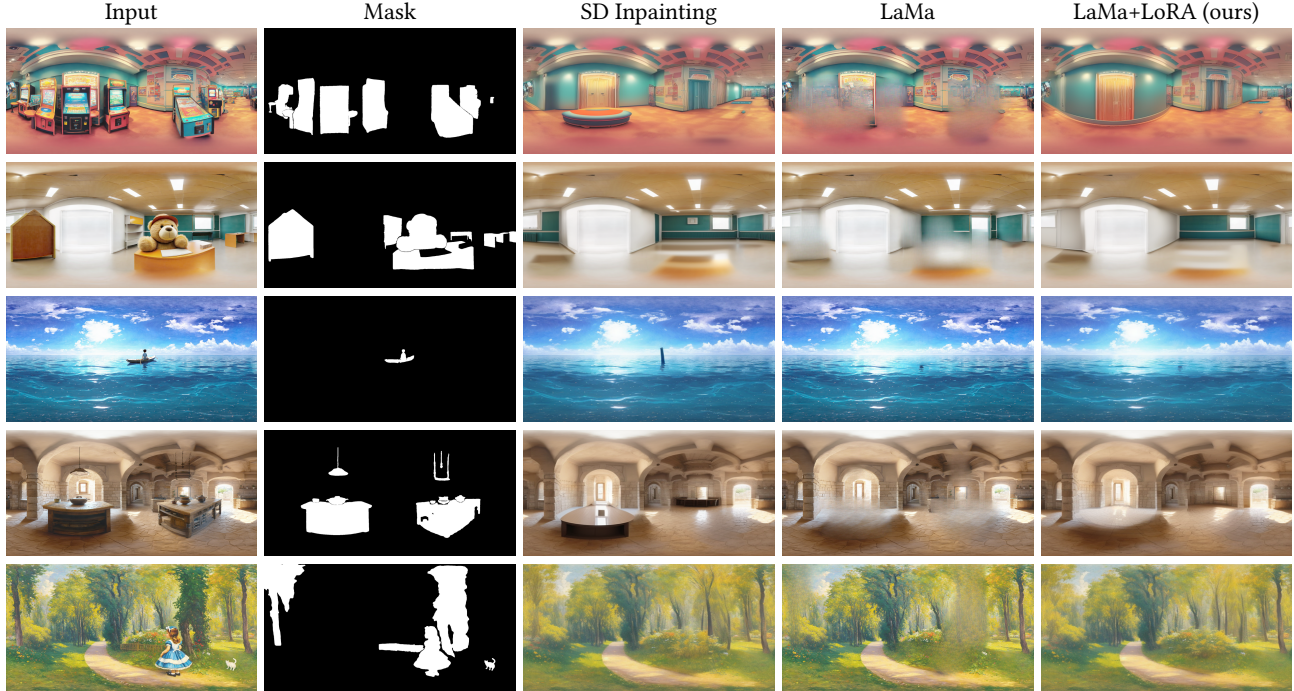


Fig. 14. Our combination of LaMa pre-inpainting and a fine-tuned LoRA outperforms both, LaMa and Stable Diffusion (SD) inpainting, delivering superior results in terms of detail and coherence. This combination enables effective inpainting for both indoor and outdoor scenes.

offset based on the minimal  $z$ -coordinate of the object’s crop in the panorama.

*Relative Pose Estimation.* The point cloud of the high-quality object  $O_{hq}$  is not guaranteed to be semantically aligned with that of the original object  $O_{crop}$  as the generated objects may vary in size and orientation. Thus, for each object, we perform an image-based relative pose estimation step that computes the relative pose between  $O_{crop}$  and  $O_{hq}$ . This process operates in two stages. First, we extract DINO [Caron et al. 2021] embeddings and compute cosine similarities between the perspective image of the cropped object ( $I_{crop}$ ) and a set of perspective projections of  $O_{hq}$  with known camera poses (the intermediate results of the object generation process described in Section C.1). Based on this we select the top  $N$  most similar reference images. We pair each of these with the image of  $O_{crop}$  and compute the relative pose using MAST3R [Leroy et al. 2024]. The final relative pose  $P_r$  is determined from the image pair with the lowest optimization loss.

## E BACKGROUND GENERATION DETAILS

To generate an initial Gaussian point cloud from the generated panorama  $I_B$  and its corresponding aligned depth map  $\tilde{D}_B$ , we first unproject the pixels into 3D positions  $\mathbf{P}$  using spherical coordinates  $\phi, \theta$  (obtained from the pixel coordinates) and depth values  $d$ :  $x = d \cos \phi \cos \theta$ ,  $y = d \cos \phi \sin \theta$ ,  $z = d \sin \phi$ . Next, the normal map  $\mathbf{N}_B$  is computed as the cross product of the partial derivatives of 3D coordinates  $\mathbf{P}$  in  $x$  and  $y$ -direction.

To keep things tractable, we sub-sample  $\mathbf{P}$ ,  $\mathbf{N}$ , and  $\mathbf{G}_B$  in spherical space: we use a uniform lat/lon lattice for horizon regions ( $|\phi| \leq 30^\circ$ ) and a Fibonacci lattice for polar regions to achieve a more uniform sampling distribution in 3D. Each sample spawns a Gaussian with:

$$\begin{aligned} \mu &= \mathbf{P}(\theta, \phi), \\ \mathbf{c} &= \text{sh}(I_B(\theta, \phi)), \\ \alpha &= 1, \end{aligned}$$

where  $\mu$  is the mean,  $\mathbf{c}$  is the RGB color encoded as a spherical harmonic and  $\alpha$  is the opacity.

Following Kerbl et al. [2023], we represent the covariance matrix as  $\Sigma = RSS^T R^T$ , where  $R$  is the rotation matrix aligning the  $z$ -axis with the normal direction, and  $S = \text{diag}(\psi, \psi, 0.01)$  encodes scale based on sampling density. We set the scale factor  $\psi$  relative to the sampling density factor ( $F_h, F_p$ ) for horizon and polar regions respectively):

$$\psi = \frac{2\pi}{2H_s} \cdot F(\phi),$$

with  $F(\phi) \in \{F_h, F_p\}$ , depending on the region and  $H_s$  the vertical sampling resolution. Experimentally, we set  $F_p = 8$  and  $F_h = 1$ .

## F 3D INPAINTING DETAILS

*Implementation Details.* After initializing the 3DGS point cloud from the panoramic image, we execute a three-stage pipeline for 3D inpainting (*Pretuning*, *Inpainting* and *Multi-view Fine-tuning*), where we use 3k/2k/2k optimization steps for the individual stages. We use MCMC-densification [Kheradmand et al. 2024] with  $\lambda_{\text{noise}} =$



Fig. 15. We reintroduce contact shadows which were removed during 2D object removal and inpainting. Simple light interaction between generated objects and the background is essential to ground the generated objects.

$5e^4$ , and also include their regularization terms for opacity and scale, with  $\lambda_o = \lambda_\Sigma = 0.5$ . For optimization on panorama reference views and inpainted images, we use a combination of  $\ell_1$ -loss, a SSIM term [Mallick et al. 2024] following Kerbl et al. [2023], as well as a  $\ell_2$ -loss against the predicted reference depth  $D_B$  to avoid overfitting to specific views and maintaining the structure of the initialization. For all views, we leverage an opacity loss, forcing the per-pixel transmittance  $T$  towards 1:

$$\mathcal{L}_{\text{img-opacity}} = \lambda_{\text{img-opacity}} \|1 - T\|^2, \quad (1)$$

with  $\lambda_{\text{img-opacity}} = 1e^3$ . To reduce noise on the final renderings, we also use a TV-loss throughout, with  $\lambda_{\text{TV}} = 1e^3$ . Finally, during *Pretuning* and *Multi-view Fine-tuning*, we reset the opacity and scale for Gaussians that are either too large or outside the scene bounds, similar to Kerbl et al. [2023]. Specifically, Gaussians are removed when  $\max(S) > 0.05 \cdot \lambda_{\text{max}}$  or  $\|\mu\| > 1.5 \cdot \lambda_{\text{max}}$ . Here,  $\lambda_{\text{max}}$  denotes our estimated scene extent, which we define as

$$\lambda_{\text{max}} = \max_{\mu_i \in \mathcal{P}_{\text{initial}}} \|\mu_i\|_\infty, \quad (2)$$

where  $\mathcal{P}_{\text{initial}}$  is the set of initial Gaussians (before inpainting). This pruning step is crucial for the elimination of elongated, disk-like Gaussians. We use LYKON/DREAMSHAPER-8-INPAINTING to inpaint the reference views, with a guidance scale of 7.5 and the same prompts as used to generate the initial panorama. The reference panorama image  $I_B$  is upscaled in two steps, first using a diffusion-based upscaler [Yang et al. 2023], followed by a non-generative one [Wang et al. 2021].

We typically use point clouds of  $\sim 4M$  points as input to the inpainting stage. We experimentally found that this offers an optimal balance between rendering efficiency, optimization performance, and sufficient density for high-quality inpainting results. The *Pretuning* stage permits a 10% increase of Gaussians for small gap filling, while the *Inpainting* step typically introduces an additional 100k Gaussians.

## G OBJECT-LIGHT INTERACTIONS

To enhance scene perception, we reintroduce light interactions removed during 2D object removal and inpainting, focusing on contact shadows, a critical cue for depth perception. Due to the lack of reliable surface normals and the absence of Gaussian raytracing in our renderer, we rely on shadow mapping to recover contact shadows, as shown in Figure 15.

As a simple heuristic for contact shadows, we generate an orthographic shadow map using a vertically positioned camera. We ignore the first layer of Gaussians which typically represents the sky or roof. We create a soft shadow mask by computing the distance to the next discontinuity in the depth map which we use during shadow evaluation to approximate a penumbra. To apply shadows to every Gaussian, we compare their positions to the shadow map, while considering a small offset due to the fuzzy nature of depth maps generated for Gaussians. We darken occluded Gaussians by mixing black into their spherical harmonics, effectively baking shadows into the representation. We also support spotlights by estimating light source locations in the panorama.

## H DETAILS OF LANGUAGE MODELS

For the high-quality object generation described in Section 3.2, we prompt GPT-4o as follows: “Describe the <object-category> in the image with a focus on its detailed attributes. Include its color, pose or orientation relative to the scene, shape, size, and material. If there is any text visible on the object, transcribe it accurately. Do not describe the background or any elements not part of the object. Be concise but complete, ensuring the total description aids accurate object reconstruction. Max 40 words.”

## I USER STUDY DETAILS

*Participant Details.* We recruited 28 participants, all with normal or corrected vision, 23-40 years old, with moderate to expert familiarity with computer graphics and vision. The study was deployed through a web interface (Google Forms) showing side-by-side video comparisons of 6s walkthroughs of the scenes. The user study first explained the criteria reported in the main text and outlined the scoring system from -2 to +2, then proceeded to show them video pairs (left and right). We did not restrict answer times, and allowed the user to watch the video repeatedly. In general, each user study lasted about  $\sim 20$  minutes and the results showed a consistent overall preference for our method. The preferences for *Coherence* and *Immersiveness* were particularly strong, while text alignment was weaker, reflecting the CLIP score in the quantitative evaluation.